

Strain distributions and electronic property modifications in Si/Ge axial nanowire heterostructures

J. G. Swadener, and S. T. Picraux

Citation: [Journal of Applied Physics](#) **105**, 044310 (2009); doi: 10.1063/1.3077293

View online: <https://doi.org/10.1063/1.3077293>

View Table of Contents: <http://aip.scitation.org/toc/jap/105/4>

Published by the [American Institute of Physics](#)

Articles you may be interested in

[VAPOR-LIQUID-SOLID MECHANISM OF SINGLE CRYSTAL GROWTH](#)

[Applied Physics Letters](#) **4**, 89 (1964); 10.1063/1.1753975

[Interface bond relaxation on the thermal conductivity of Si/Ge core-shell nanowires](#)

[AIP Advances](#) **6**, 015313 (2016); 10.1063/1.4940768

[Si/Ge hetero-structure nanotube tunnel field effect transistor](#)


[Journal of Applied Physics](#) **117**, 014310 (2015); 10.1063/1.4905423

[Nature of heterointerfaces in GaAs/InAs and InAs/GaAs axial nanowire heterostructures](#)

[Applied Physics Letters](#) **93**, 101911 (2008); 10.1063/1.2978959

[One-dimensional heterostructures in semiconductor nanowhiskers](#)

[Applied Physics Letters](#) **80**, 1058 (2002); 10.1063/1.1447312



Contact Hiden Analytical for further details:
www.HidenAnalytical.com
info@hiden.co.uk


CLICK TO VIEW our product catalogue

Instruments for Advanced Science




Gas Analysis

- dynamic measurement of reaction gas streams
- catalysis and thermal analysis
- molecular beam studies
- dissolved species probes
- fermentation, environmental and ecological studies



Surface Science

- UHV TPD
- SIMS
- end point detection in ion beam etch
- elemental imaging - surface mapping



Plasma Diagnostics

- plasma source characterization
- etch and deposition process reaction kinetic studies
- analysis of neutral and radical species



Vacuum Analysis

- partial pressure measurement and control of process gases
- reactive sputter process control
- vacuum diagnostics
- vacuum coating process monitoring

Strain distributions and electronic property modifications in Si/Ge axial nanowire heterostructures

J. G. Swadener^{a)} and S. T. Picraux

Center for Integrated Nanotechnologies, Los Alamos National Laboratory, Los Alamos, New Mexico 87545, USA

(Received 19 June 2008; accepted 3 January 2009; published online 26 February 2009)

Molecular dynamics simulations were carried out for Si/Ge axial nanowire heterostructures using modified effective atom method (MEAM) potentials. A Si–Ge MEAM interatomic cross potential was developed based on available experimental data and was used for these studies. The atomic distortions and strain distributions near the Si/Ge interfaces are predicted for nanowires with their axes oriented along the $[111]$ direction. The cases of 10 and 25 nm diameter Si/Ge biwires and of 25 nm diameter Si/Ge/Si axial heterostructures with the Ge disk 1 nm thick were studied. Substantial distortions in the height of the atoms adjacent to the interface were found for the biwires but not for the Ge disks. Strains as high as 3.5% were found for the Ge disk and values of 2%–2.5% were found at the Si and Ge interfacial layers in the biwires. Deformation potential theory was used to estimate the influence of the strains on the band gap, and reductions in band gap to as small as 40% of bulk values are predicted for the Ge disks. The localized regions of increased strain and resulting energy minima were also found within the Si/Ge biwire interfaces with the larger effects on the Ge side of the interface. The regions of strain maxima near and within the interfaces are anticipated to be useful for tailoring band gaps and producing quantum confinement of carriers. These results suggest that nanowire heterostructures provide greater design flexibility in band structure modification than is possible with planar layer growth. © 2009 American Institute of Physics. [DOI: [10.1063/1.3077293](https://doi.org/10.1063/1.3077293)]

I. INTRODUCTION

Semiconductor nanowires have received increasing interest for electronic, photonic, and thermoelectric applications because of their potential for integration into high density three-dimensional microelectronic devices. For the past 25 years, band-gap engineering has been accomplished by using epitaxial semiconductor films on substrates to produce quantum wells, strained-layer superlattices, and other two-dimensional structures with planar interfaces. However, misfit dislocations, other interface defects, and surface morphology changes limit the thicknesses and strains that can be achieved by this approach.^{1–4} Extended defects in semiconductors leave dangling bonds, which cause deep levels in the energy gap and act as carrier traps.^{5,6} In addition, defects can act as traps for impurities and dopants. In contrast, Si/Ge nanowire structures can be constructed without extended defects^{7,8} and have the potential to tune the Si/Ge band offsets and to achieve an unprecedented level of modification to the Ge band gap. The large aspect ratio of nanowires permits strain relief in two dimensions as a result of the traction-free surfaces, which is anticipated to allow Si/Ge axial nanowire heterostructures to remain free of extended defects at sizes much larger than for planar structures where the layers are laterally confined. In addition and as we will show, the anisotropy of the crystal structure results in unexpected variations in strain and strain localizations in regions that are

smaller than the Bohr radius in Ge ($r_0 \sim 8$ nm for Ge and ~ 3 nm for Si) and are therefore expected to induce quantum confinement.

There have been only a limited number of theoretical or simulation studies of strain distributions and the influence of the strain in semiconducting nanowires and nanowire heterostructures. Molecular dynamics (MD) simulations of mechanical properties have been carried out for 4 nm diameter Si nanowires using Stillinger–Weber potentials.⁹ MD simulations have also been used to compare the accuracy of Tersoff and Stillinger–Weber potentials for simulating surface reconstructions on ~ 3 nm diameter Si nanowires.¹⁰ Strain-driven effects on electronic properties have been examined for monoatomic Si and for InAs/GaAs nanowire superlattices using the empirical tight-binding method for diameters of 20 nm¹¹ and for monoatomic Si nanowires using density functional theory for diameters ≤ 4 nm.¹² Studies of strained axial interfaces have been primarily limited to axisymmetric analytical or finite element methods to determine the strain distributions or strain energy and to predict the equilibrium size limits for coherency at these interfaces.^{13–16} For metal nanowires the combined use of MD simulations together with embedded atom method (EAM) potentials has allowed much larger diameter metallic nanowires to be simulated for modeling of their strain, deformation, and other mechanical properties.¹⁷

In this work we examine the deformation and strain produced in selected cases for axial Si/Ge nanowire heterostructures (referred to as biwires) and for the case of a thin Ge disk sandwiched within a Si nanowire (two biwire inter-

^{a)}Electronic mail: swadener@lanl.gov.

TABLE I. MEAM parameters for Ge, Si, and Si-Ge potentials: sublimation energy E^0 (eV), equilibrium nearest neighbor distance R^0 (Å), cutoff radius r_c (Å), distance at which partial screening begins c_{\min} and ends c_{\max} (Å), exponential decay factor α , cubic term strength δ for the universal energy function, scaling factor for the embedding energy A , exponential decay factors for the atomic densities $\beta^{(i)}$, weighting factors for the atomic densities $t^{(i)}$, and the atomic electron density weights ρ_0 .

	E^0	R^0	r_c	c_{\min}	c_{\max}	α	δ	A	$\beta^{(0)}$	$\beta^{(1)}$	$\beta^{(2)}$	$\beta^{(3)}$	$t^{(0)}$	$t^{(1)}$	$t^{(2)}$	$t^{(3)}$	ρ_0
Ge	3.85	2.448	4.0	2.0	2.8	4.98	0	1.0	4.55	5.5	5.5	5.5	1	4.02	5.23	-1.6	0.88
Si	4.63	2.35	4.0	2.0	2.8	4.87	0	1.0	4.4	4.9	5.5	5.5	1	2.25	4.47	-1.8	1.0
Si-Ge		2.361	4.0	2.0	2.8	5.60	0.05										

faces). By using MD modeling we are able to carry out a complete strain analysis at the atomic level, incorporating crystal structure, anisotropy, Si-Ge atomic bonding across the Si/Ge interface, traction-free surfaces, and surface reconstructions. Further, by exploiting modified embedded atom method (MEAM) potentials previously developed for Si and Ge, and by developing a Si-Ge cross potential in these MD simulations, we are able to extend these interfacial axial heterostructure studies to realistic nanowire diameters of 10 to 25 nm. From the MD results, we map the magnitude and extent of the strain, identify the areas of strain localization, and estimate the band-gap modifications using deformation potential theory.^{18–20}

II. METHODS

Our investigation uses MD with Si, Ge, and Si-Ge cross potentials derived using the MEAM.²¹ The MEAM potentials have been previously developed for Si and Ge (Refs. 22 and 23) to allow the realistic inclusion of directional effects. The parameters for the potentials are listed in Table I. The original MEAM Ge potential²² and a slight modification²³ of the previous MEAM Si are used.

The original MEAM Si potential²² gave a relaxed vacancy formation energy of 2.84 eV, which is below the experimental values (Watkins and Corbett²⁴ gave 3.6 ± 0.5 eV and Dannafer *et al.*²⁵ gave 3.6 ± 0.2 eV) and *ab initio* calculations (3.5–4.1 eV, see Ref. 26). Therefore, the MEAM potential was modified: $\beta^{(1)}$ was changed from 5.5 to 4.8 and $t^{(1)}$ was changed from 3.13 to 2.75 (see Table I), which increased the relaxed vacancy formation energy to 3.40 eV. The elastic constants determined for Si using this modified potential are $C_{11}=164$ GPa, $C_{12}=69.5$ GPa, and $C_{44}=86.3$ GPa, which are close to those for the original potential and within 10% of the experimental values ($C_{11}=165.7$ GPa, $C_{12}=63.9$ GPa, and $C_{44}=79.7$ GPa).²⁷ We note that the often used Stillinger-Weber potential²⁸ for Si gives elastic constants which are 20% lower than the experimental values. Surface energies given by the modified potential are 1.33 J/m² for the unreconstructed Si (111) surface, 1.56 J/m² for the unreconstructed (110) surface, and 2.0 J/m² for the 2×1 reconstructed (100) surface, which are still close to the range of experimental values [Gilman²⁹ gave 1.24 J/m² for the (111) surface; Jacodine³⁰ gave 1.23 J/m² for the (111) surface, 1.51 J/m² for the (110) surface, and 2.13 J/m² for the (100) surface]. The Si and Ge MEAM potentials employed here have been widely used and have predicted various structures with accuracies of 2%–5% [see, for example, Refs. 21–23 even for the case where local

strains have exceeded 10%]. Models of pure Si nanowires that use this Si MEAM potential are in good agreement with experimental observations. The MEAM models show a transition from (111) stable axial Si wires at large diameters to stable (211) wires as the diameter is decreased to 20 nm compared to 20–30 nm in experiments.³¹ In addition, faceted sides are found to be stable in small Si nanowires that are hydrogen passivated, while unpassivated nanowires are round, in agreement with experiments.^{31,32}

The Si-Ge cross potential parameters were derived in this work by obtaining optimal results for Ge adatom diffusion on a (100) Si surface while maintaining a reasonable fit to the elastic constants for a random mixture SiGe alloy. For consistency, the cutoff radius (r_c) and the shielding parameters (c_{\min} , c_{\max}) were kept fixed at the same values as used for the Si and Ge potentials. The value of the cubic term strength $\delta(1,2)$ was fixed at 0.05 eV to match the heat of mixing.^{33,34} The remaining terms for the Si-Ge cross potential (R^0 , α , and the ratio of the ρ_0 values for Si and Ge) were varied to achieve an optimal fit to both the elastic constants of the SiGe alloy and the Ge adatom diffusion on a 2×1 reconstructed (100) Si surface. This procedure amounts to an effort to obtain an optimal fit to four experimental values using three fitting parameters.

For the Si MEAM potential, the (100) Si surface relaxes directly to the 2×1 reconstruction, in agreement with experimental observations. Island growth experiments of Ge on a 2×1 (100) Si surface have shown that diffusion of Ge adatoms is preferential in the direction of the 2×1 channels.^{35,36} There are two potential paths for diffusion along the channel direction, which we will call a_{\parallel} and b_{\parallel} and also two potential paths for diffusion perpendicular to the channel directions, which we will call a_{\perp} and b_{\perp} . The detailed paths are defined in Ref. 33 as $A \rightarrow D \rightarrow G \rightarrow (D) \rightarrow (A)$ for a_{\perp} , $A \rightarrow D \rightarrow F \rightarrow G \rightarrow (D) \rightarrow (A)$ for b_{\perp} , $F \rightarrow G \rightarrow (F)$ for a_{\parallel} , and $F \rightarrow D \rightarrow G \rightarrow (F)$ for b_{\parallel} . For the potential that we have derived (Table I), paths a_{\perp} and b_{\perp} have the same barrier to diffusion, while paths a_{\parallel} and b_{\parallel} have lower barriers than a_{\perp} and b_{\perp} , but different barrier heights. Our potential shows that path a_{\parallel} is favorable by 0.07 eV, and path b_{\parallel} is favorable by 0.13 eV, compared to paths a_{\perp} and b_{\perp} . For island growth, paths a_{\parallel} and b_{\parallel} should be almost equally likely, because the Ge adatom is equally likely to move $F \rightarrow D$ or $F \rightarrow G$ and thus will start out along either path. Therefore, diffusion is preferentially along the 2×1 channels by an average of 0.10 eV, in qualitative agreement with the experimental observations of preferential island growth.³⁶ For diffusion of Si adatoms on 2×1 (100) Ge surface, our

TABLE II. Elastic constants (GPa) for a random SiGe alloy determined with the MEAM potentials from Table I.

	MEAM	Expt. ^a
C_{11}	161.6	161
C_{12}	68.6	83.5
C_{44}	91.1	85.5

^aReference 31.

Si–Ge cross potential also predicts preferential diffusion parallel to the 2×1 channel direction, in agreement with previous results.^{35,36}

The three elastic constants for a SiGe random alloy obtained using our derived potentials are compared with the experimental results³³ in Table II. Better fits to the elastic constants resulted in a worse fit to the Ge adatom diffusion, so this potential was chosen as the best compromise for fitting both diffusion and elastic constant results. The value for C_{12} using our potential is 18% low, while the value of C_{44} is 6.5% high and the value of C_{11} is within 0.5%. This fit to the elastic constants is relatively good and better than that obtained for the individual monoatomic cases using Stillinger–Weber potentials. Cross potentials are inherently more difficult to fit than the potentials for monoatomic systems and the present fit is better than previously obtained for Si–Ge cross potentials.³⁵

MD simulations used the LAMMPS (Ref. 37) parallel MD code running on 8–32 processors with the number of atoms ranging from 0.1×10^6 to 1.7×10^6 . Energy was minimized using the conjugate gradient method with a tolerance of 10^{-7} . Relaxed atomic positions were used in all calculations. For adatom diffusion barrier calculations, the surface was relaxed and the adatom was added at different locations and allowed to relax in the vertical direction, while holding its lateral position fixed. The barrier heights were determined from the energy increase at the saddle position between two local minima. Models of Si/Ge biwires with coherent, atomically sharp interfaces were constructed to evaluate the strains that would be generated in axial heterostructures. Ideal interfaces with no mixing are difficult to achieve experimentally for Si/Ge nanowires by the usual vapor-liquid-solid growth technique due to the residual Si or Ge solute remaining in the liquid upon switching between Si and Ge growth. However, our MD results should serve as a basis to evaluate the potential effects that could be achieved for such interfaces and to motivate the continued improvement for the Si/Ge experimental system. The MD models also provide a baseline for comparison of future experimental or atomistic results with interface mixing. Typical MD models are shown in Fig. 1. Figure 1(a) illustrates a 10 nm diameter \times 30 nm tall [111] Si/Ge biwire, and Fig. 1(b) shows a 25 nm diameter nanowire structure with a 1 nm thick layer of Ge disk embedded in a 75 nm tall [111] Si nanowire. A third model system used in this study was a 25 nm diameter \times 75 nm tall [111] Si/Ge biwire.

III. RESULTS AND DISCUSSION

In the present studies, we have calculated the atom positions and the strains for Si/Ge axial heterostructures for

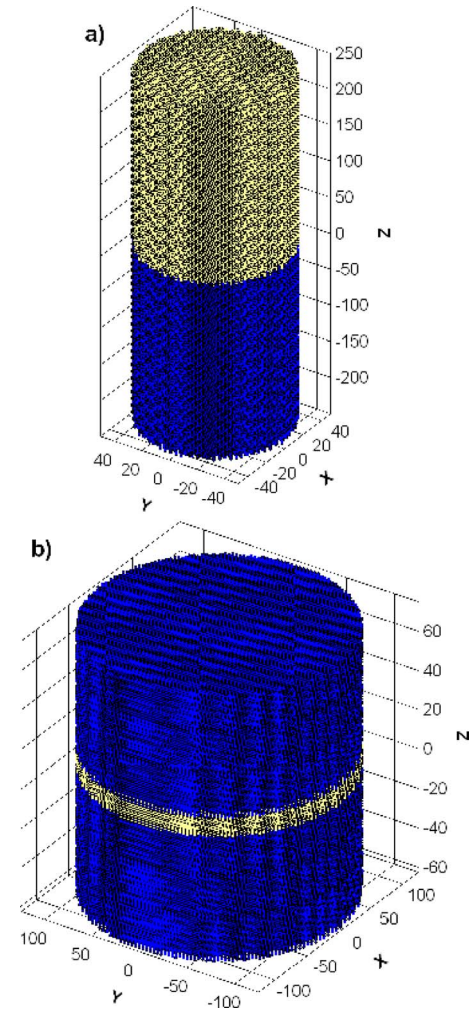


FIG. 1. (Color online) Structures used in the MD calculations: (a) 10 nm diameter Si/Ge axial heterostructure (biwire); (b) axial heterostructure with a 1 nm thick Ge (yellow) layer sandwiched in a 25 nm diameter Si (blue) nanowire (all dimensions in Å). The z direction corresponds to the nanowire axis and is taken to be along the [111] crystal orientation in these studies.

nanowires oriented along the [111] direction. Figure 2 shows the positions of the Ge atoms immediately adjacent to the Si/Ge interface (referred to as the Ge interface atoms) for the 10 nm diameter Si/Ge biwire. For clarity, the outermost atom

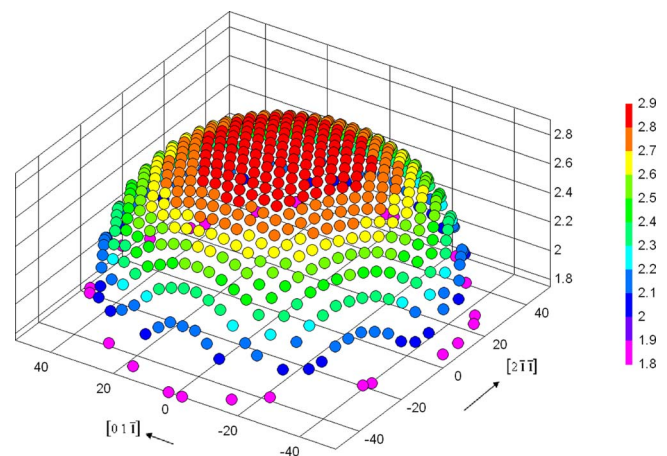


FIG. 2. (Color online) Height profile of Ge interface atoms in a 10 nm diameter [111] Si/Ge biwire (all dimensions in Å).

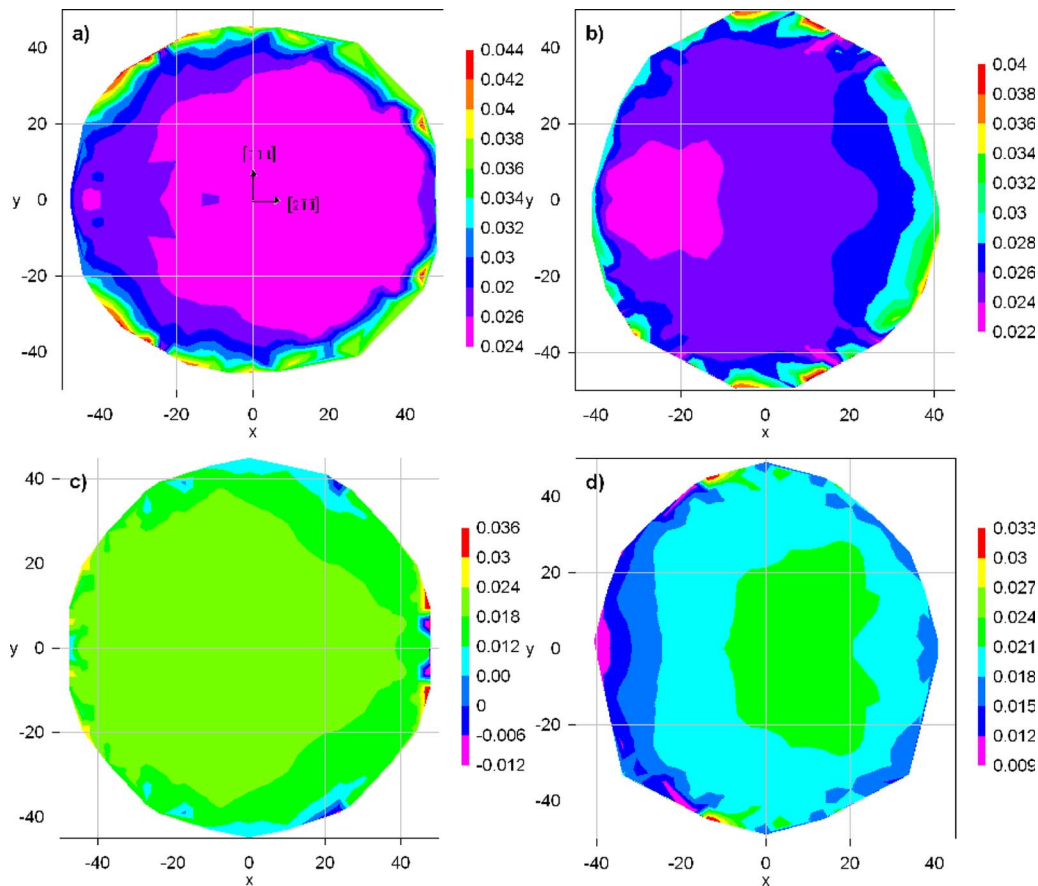


FIG. 3. (Color online) Contour plots of in-plane strains in a 10 nm diameter Si/Ge biwire where the x and y axes correspond to the $[2\bar{1}\bar{1}]$ and the $[01\bar{1}]$ directions, respectively, and the z axis corresponds to the $[111]$ direction: (a) ε_{yy} in the Ge interfacial layer, (b) ε_{xx} in the Ge interfacial layer, (c) ε_{yy} in the Si interfacial layer, and (d) ε_{xx} in the Si interfacial layer. (All strains are referenced to the Si lattice and all dimensions are in Å.)

layer around the nanowire is not shown in Fig. 2, because those atoms move to locations based on the specific termination of the surface as a result of surface reconstructions. Thus the locations of those atoms are a surface effect and not due to the heterostructure strain. Similarly the strain plots shown in Fig. 3 and subsequent figures do not show the strains between an outermost atom and an atom adjacent to it, because the positions of the outermost atoms are a surface effect and do not give a useful result for strain. From Fig. 2 it is apparent that a substantial two-dimensional bowing of the nanowire interface occurs, with the positions of the Ge atoms curved downward in the outer regions toward the Si nanowire. A similar curvature would be observed for a bilayer where Ge has the larger lattice constant. The relative displacements for this case of a 10 nm diameter biwire reach ~ 0.1 nm in the Ge interfacial layer.

Figure 3(a) shows a contour plot of the ε_{yy} strain corresponding to the $[01\bar{1}]$ direction (y -direction in the plot) for the interfacial layer of Ge atoms (those Ge atoms immediately adjacent to the Si/Ge interface) in a 10 nm diameter Si/Ge biwire. Figure 3(b) shows the ε_{xx} strain corresponding to the $[2\bar{1}\bar{1}]$ direction (x -direction in the plot) for the same interfacial layer of Ge atoms. The ε_{yy} strains in the $[01\bar{1}]$ direction for the Si atoms on the opposite side of the interface are plotted in Fig. 3(c), and the ε_{xx} strains in the $[2\bar{1}\bar{1}]$ direction for the Si interface atoms are plotted in Fig. 3(d).

All the strains shown are relative to the Si lattice for consistency and the strains are tensile for Si. The strains relative to the Ge lattice can be determined by subtracting 0.041 from the strain values shown, which gives compressive strains for Ge.

The strains, as seen in Fig. 3, are asymmetric in reflection about the $(2\bar{1}\bar{1})$ plane because of the diamond lattice stacking sequence and the mismatch in elastic constants across the Si/Ge interface. This asymmetry can be easily seen by viewing the three-dimensional diamond lattice crystal structure, because the Si/Ge interface occurs at only one plane in the ABC stacking sequence in the $[111]$ axial direction. A single (111) Ge layer contains threefold symmetry, but the layer above it is offset in the $[2\bar{1}\bar{1}]$ direction. The strains show symmetric reflection about the central $(01\bar{1})$ plane, because the central $(01\bar{1})$ plane is a plane of symmetry for the entire biwire. In the Ge interfacial layer, the maximum compressive ε_{xx} strain is 0.020 and occurs at $(x,y) = (-2.0 \text{ nm}, 0 \text{ nm})$, and the maximum compressive ε_{yy} strain is 0.018 and occurs at $(x,y) = (1.0 \text{ nm}, 0 \text{ nm})$, but the maximum combined average in-plane strain $(\varepsilon_{xx} + \varepsilon_{yy})/2$ is 0.019 and occurs at $(x,y) = (-1.8 \text{ nm}, \pm 1.0 \text{ nm})$. The combined average in-plane stress maxima result in two minima in the band gap in the strained Ge interface layer at $(-1.8 \text{ nm}, \pm 1.0 \text{ nm})$.

The large strains predicted for the axial heterostructures will have a significant influence on the band structure. We first summarize the nature of these effects qualitatively and then predict the magnitude of their influence on the band gaps using deformation potential theory. In Ge the minimum in the conduction band falls along the $[111]$ axis of the Brillouin zone, whereas for Si the conduction band minimum lies near the $[100]$ axis of the Brillouin zone. Therefore, for Ge, in-plane compression stress in the $[111]$ nanowires cause out-of-plane tensile strain, which leads to conduction band splitting at the L point and relatively large band-gap changes. In contrast, for Si strain in the $[111]$ direction does not lead to splitting of the minimum conduction bands which is near the X point. Valence band splitting occurs for both Si and Ge due to lifting of the degeneracy at the Γ point. The v_2 band (Γ'_{25}) remains the highest valence band in Ge for nanowires in the $[111]$ orientation, whereas for Si the v_1 band becomes the highest valence band. A significant spin-orbit splitting is present in the valence band of 0.3 eV for Ge and 0.044 eV for Si. The strain contribution to this splitting is relatively small.³⁸ There is an additional small increase in the average valence band energy as a result of compressive hydrostatic stress. Thus the influence of strain on the Si/Ge nanowire band structure near the interface for the $[111]$ axial heterostructures is expected to be significant.

Using deformation potential theory,^{18–20,38} one can estimate the band gaps in the linear strain-dependent limit. The relative effect of strain on the band gap will be greatest for Ge because of its smaller unstrained band gap (0.74 eV) and the larger spin-orbit splitting. For in-plane strain in the (111) plane, the maximum band-gap reduction from deformation potential theory is

$$\Delta E_G = -\frac{1}{3}\Delta_0 + \left(\frac{1}{4}\delta E_{111} - \frac{1}{3}\Xi_u^L\right)(2\varepsilon_{zz} - \varepsilon_{xx} - \varepsilon_{yy}) - \delta E_H(\varepsilon_{zz} + \varepsilon_{xx} + \varepsilon_{yy}), \quad (1)$$

where Δ_0 is the spin-orbit splitting in the valence band, δE_{111} is the deformation potential in the $[111]$ direction, Ξ_u^L is the band-gap reduction resulting from the conduction band splitting in the $[1\bar{1}\bar{1}]$, $[\bar{1}1\bar{1}]$, and $[\bar{1}\bar{1}1]$ bands at the L point, and δE_H is the hydrostatic component of the change in the band gap. The shear strains are <0.001 , which is small compared to the normal strains, and thus their effect on band offsets can be neglected to first order. Using the experimental values of $\Delta_0=0.3$ eV, $\delta E_{111}=-18.4$ eV, $\Xi_u^L=16.2$, and $\delta E_H=-2.0$ eV,^{38,39} the band gap in Ge at the two strain maxima at the biwire interface would be reduced by ~ 0.27 eV relative to unstrained Ge. At the nearby (x,y) position of $(-1.8, 0)$, the average combined in-plane strain is 0.018 and the corresponding local change in band-gap energy is estimated to be ~ 0.26 eV, or 0.010 eV higher than the minimum. The average in-plane strain decreases to 0.014 at $(0, 0)$, which would be expected to result in a band gap about 0.043 eV greater than the band gap at the maximum strain points. Such local strain maxima and the resulting band energy localizations suggest that it may be possible to confine carriers within local regions at the Si/Ge interface of nanowires at low temperatures. Further electronic structure calculations

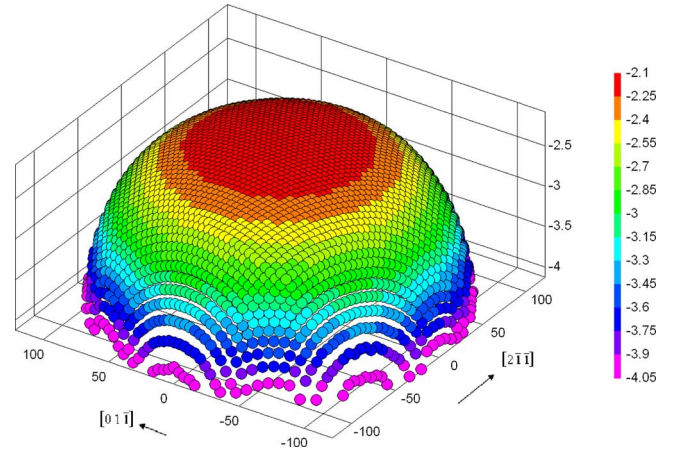


FIG. 4. (Color online) Height profile of Ge interface atoms in a 25 nm diameter Si/Ge biwire. (All dimensions are in Å.)

and experimental studies are needed to confirm this prediction.

Figure 4 shows the positions of the Ge interface atoms for a 25 nm diameter Si/Ge biwire. While the absolute value of the strain-induced change in height of the Ge atoms is seen to vary by about 0.2 nm from the center to the outer region at the nanowire interface, which is greater than for the 10 nm nanowire (see Fig. 2), the curvature of the 25 nm biwire interface is not as great as for the 10 nm biwire. Specifically, for a 2.5 factor increase in diameter, the maximum displacement increases only by approximately a factor of 2 and thus greater distortions are found at the axial heterostructure interface as the nanowire diameter decreases. For both the 10 and 25 nm diameter nanowires, the local distortions approximately mimic the symmetry of the (111) plane, although the exact atomic displacements show asymmetry about the $(2\bar{1}\bar{1})$ plane.

The strain distributions for the Ge and Si atoms adjacent to the interface for the 25 nm diameter biwire case are shown in Fig. 5. The strain distributions are again seen to be axially asymmetric. The maximum strains in the 25 nm biwires are slightly greater than in the 10 nm biwire, but the localization is not as strong. A localized region of maximum strain is still observed in the Ge interface layer [see Fig. 5(b)] approximately in the region from $-11 < x < -7$ nm and $-4 < y < 4$ nm, where the Ge compressive strain exceeds -0.022 , which corresponds to an estimated decrease in the Ge band gap of ~ 0.29 eV. While this region is larger than the localized region in the 10 nm biwire, it is still comparable to the Bohr radius in Ge (~ 8 nm), and therefore would be expected to show possible quantum confinement effects. The MEAM potentials used to calculate the strain in these MD studies with $>1 \times 10^6$ atoms are not able to predict quantum confinement effects nor the direct-indirect transition that has been predicted for Si nanowires with very small diameters (1–7 nm) (Refs. 40–43) and in Ge layers strained in tension.⁴⁴ These potentials can only be used to give the strain and atom positions, which can then be used as inputs to more sophisticated atomistic models. However, we note that those more detailed models such as density functional theory, pseudopotential, or tight-binding methods are limited to

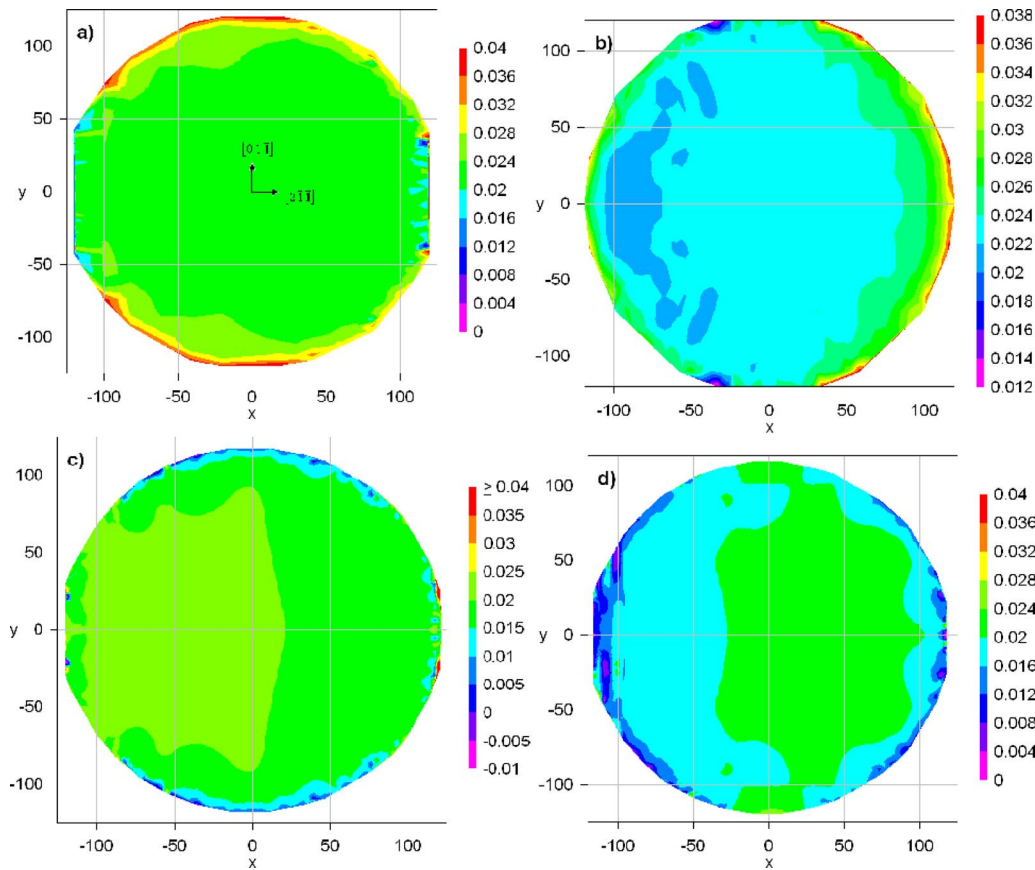


FIG. 5. (Color online) Contour plots of in-plane strains for a 25 nm diameter Si/Ge biwire where the x and y axes correspond to the $[2\bar{1}\bar{1}]$ and the $[01\bar{1}]$ directions, respectively: (a) ϵ_{yy} in the Ge interfacial layer, (b) ϵ_{xx} in the Ge interfacial layer, (c) ϵ_{yy} in the Si interfacial layer, and (d) ϵ_{xx} in the Si interfacial layer. (All strains are referenced to the Si lattice and all dimensions are in Å.)

much smaller numbers of atoms, and as a result have not been applied to nanowires above ~ 5 nm in diameter.

A comparison of the ϵ_{xx} strains along the x -axis in the biwires with different diameters is shown in Fig. 6(a). In this plot the strains for the Si and Ge atoms on either side of the biwire interface are referenced to unstrained Si and Ge, respectively, and thus the ordinate corresponds to tensile stress for the Si interface atoms and compressive stress for Ge interface atoms. Localized regions with changes in strain of about 0.2%–0.3% can be seen in both the Si and Ge layers. For the Si interfacial layer, a maximum occurs in the tensile ϵ_{xx} strain near the middle of the 10 nm biwire, while the 25 nm biwire has a broad plateau of strain with almost the same value as the maximum tensile strain for the 10 nm diameter nanowire. For the Ge interfacial layers, the peak of localized compressive strain is seen to occur near the outer region of one side of the biwire for both the 10 and 25 nm diameter cases. The localized strain maxima observed in the interface layers are confined to just the interfacial atomic layers and decrease sharply with distance from the interface.

In contrast to the biwire case, the Si/Ge/Si axial heterostructures with a thin 1 nm Ge layer exhibit very little distortion at the Si/Ge interfaces. Figure 7 shows a plot of the height profile of one of the Ge interfacial layers in a 25 nm diameter Si/Ge/Si nanowire with a 1 nm thick Ge layer. As shown in Fig. 7, the interior Ge interface atoms remain in a band 50 pm thick, and except for an outer ring approximately

4 atoms wide, the Ge interface atoms are in a very flat layer with a height variation of less than 4 pm. The in-plane strains for this Ge interface layer are shown in Fig. 8. For this case, both interfaces have similar strain profiles, and the strain is approximately uniform through the 1 nm thick Ge layer. A relatively large region of in-plane compressive biaxial strain >0.035 exists approximately centered in the Ge layer. In Fig. 6(b), it can be seen more clearly that the strain in the Ge and Si interfacial layers is asymmetric, as was found for the biwire cases.

The biaxial strain of approximately 0.035 [see Fig. 6(a)] predicted for this Ge disk within the Si nanowire is a large fraction of the lattice mismatch of 0.041, indicating that $>85\%$ of the strain in the central region is incorporated into the thin Ge disk. From deformation potential estimates, this compressive strain corresponds to a reduction in the Ge band gap in the central region of approximately 0.4 eV, which is a large percentage of the bulk Ge band gap (0.74 eV). Regions with significant strain localization are not produced in the interior of the Ge layer, in contrast to the biwire case. Some strain localization may be present near the outer edge of the nanowire interfaces, although this is less certain since these regions may be influenced by specific surface atom terminations and reconstructions. As shown in Fig. 6(b), tensile ϵ_{xx} strains in the Si interface layer for the Si/Ge/Si heterostructure are relatively small, except for near the edge where they reach ~ 0.02 . Thus the strain is nearly equally shared across

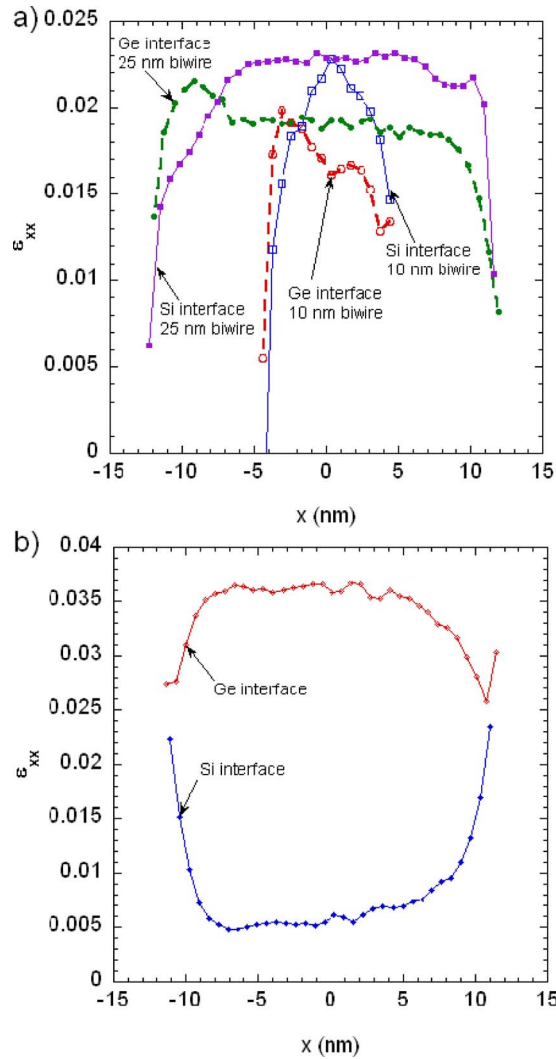


FIG. 6. (Color online) Comparison of ϵ_{xx} strains (shown are tensile strains for Si and compressive strains for Ge) in the $[2\bar{1}\bar{1}]$ direction at the Si/Ge interfaces in (a) 10 and 25 nm diameter Si/Ge biwires and (b) a Si/Ge/Si heterostructure for a 25 nm diameter nanowire with the Ge layer 1 nm thick.

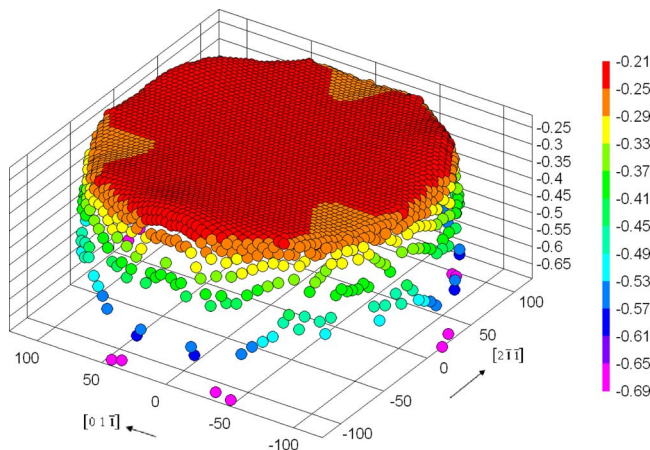


FIG. 7. (Color online) Height profile of Ge interface atoms in a 25 nm diameter Si/Ge/Si heterostructure with the Ge layer 1 nm thick. (All dimensions are in Å.)

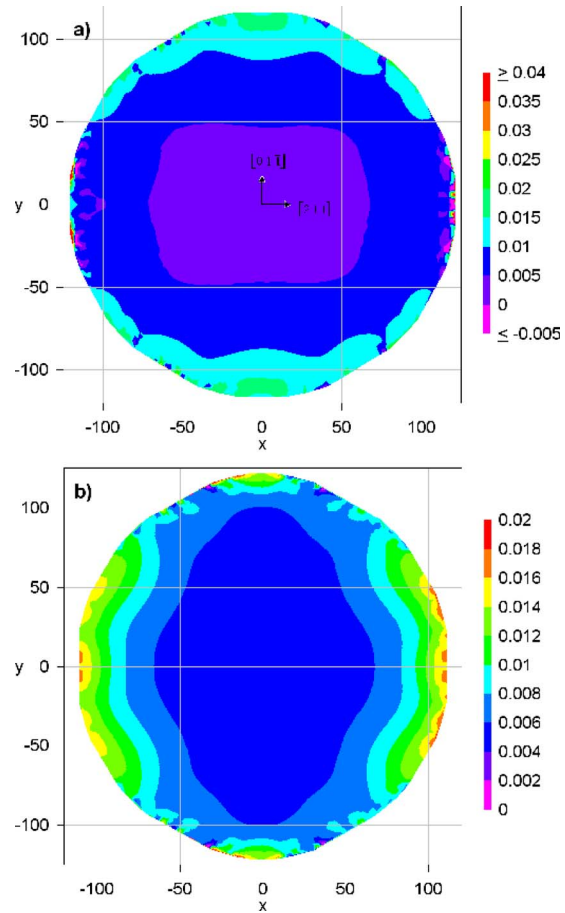


FIG. 8. (Color online) Contour plots of in-plane strains for a 1 nm thick Ge layer sandwiched in a 25 nm diameter Si nanowire where the x and y axes correspond to the $[2\bar{1}\bar{1}]$ and the $[01\bar{1}]$ directions, respectively: (a) ϵ_{yy} in the Ge interface layer and (b) ϵ_{xx} in the Ge interface layer, where the interface resides on a shuffle plane. (All strains are referenced to the Si lattice and all dimensions are in Å.)

the interface for the biwire case, but is largely confined to the thin Ge layer for the Si/Ge/Si heterostructure case. It is also of interest to examine the change in strain along the nanowires as a function of distance from the interface. As would be expected, the largest strains occur at the interfacial layers and the magnitude of the strains is shown to decrease rapidly with distance from the interface as seen in Fig. 9. For clarity, only ϵ_{yy} strains for the 10 and 25 nm diameter nanowires are shown in Fig. 9, but the variation in ϵ_{xx} strains with distance from the interface is similar. For the biwires, the strains are found to decrease with distance from the interface at a rate proportional to the diameter of the biwire, decreasing to an approximately unstrained level at a distance of $\sim 0.3d$. The strain further decreases to a minimum slightly less than zero, which reflects the fact that equilibrium must be maintained throughout the nanowire. The strain variation in Si and Ge are similar, except that the magnitude of the strains in Si away from the interface is slightly larger. For the Si/Ge/Si heterostructure, the magnitude of the strains in Si near the interface is not as large since the strain has been largely shifted to the Ge disk in this case, and the strain in the Si decreases to zero over about the same normalized distance of $z/d \approx 0.3$. A Si/Ge/Si heterostructure with a thicker Ge layer

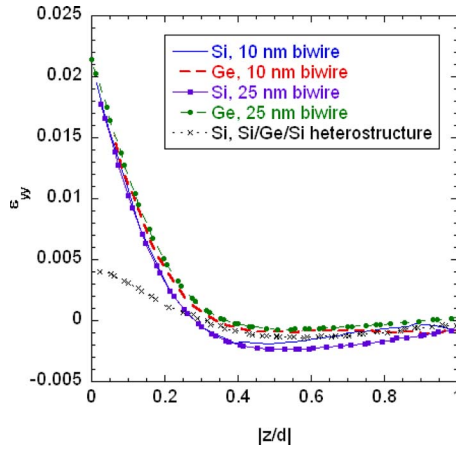


FIG. 9. (Color online) Variation in ε_{yy} strains in the $[01\bar{1}]$ direction with distance from the Si/Ge interfaces in the z direction divided by the nanowire diameter, d , in 10 and 25 nm diameter Si/Ge biwires and in the 25 nm diameter Si/Ge/Si heterostructure. Note that the values are given as tensile strains for Si and compressive strains for Ge.

would result in larger strains in Si and a faster decrease in strain, with a similar scaling with distance from the interface anticipated.

The rapid decrease in strain with distance from the interface for the Si/Ge biwire results in the minimum in the Ge band gap being localized in the region near the heterostructure interface. Using deformation potential theory, we can estimate the nature of this localization. The approximate band edge behavior at the center of the 25 nm Si/Ge nanowire based on deformation potential theory^{18–20,38} is shown schematically in Fig. 10(a). The calculations employ recent experimental results for the Si conduction band deformation potential⁴⁵ as well as earlier results for the Si valence band⁴⁶ and for Ge.^{38,39} Here the v_2 band in Ge is taken to be 0.54 eV above the v_1 band in Si based on *ab initio* calculations.⁴⁷ An electron well approximately 0.12 eV deep is observed in Si at the interface relative to Si far from the interface. In Ge the electron well at the interface is approximately 0.14 eV relative to Ge far from the interface and is located 0.05 eV higher than the Si electron well. However, the exact relative positions would change as a result of band bending, which depends on the specific Fermi level of the two materials. For holes a corresponding significant confinement is expected, with the holes being confined on the Ge side of the interface [see Fig. 10(a)].

The Si/Ge/Si heterostructure with a 1 nm Ge layer is expected to have an even deeper carrier confinement than for the biwire, because the strain is primarily transferred to the Ge region. From deformation potential theory, an electron well depth of 0.15 eV and a hole well of 0.69 eV are found in the Ge layer, as shown in Fig. 10(b). These deformation potential theory calculations are based on experimental results, which employed strains of up to 0.014 for uniaxial compression,³⁸ and also some of the experimentally determined values depend on curve fits to quadratic effects. Since the strains found here for Si/Ge axial heterostructures are significantly greater, these extrapolations of the deformation potentials must be considered approximate. However, our results indicate the presence of large strain-induced effects on

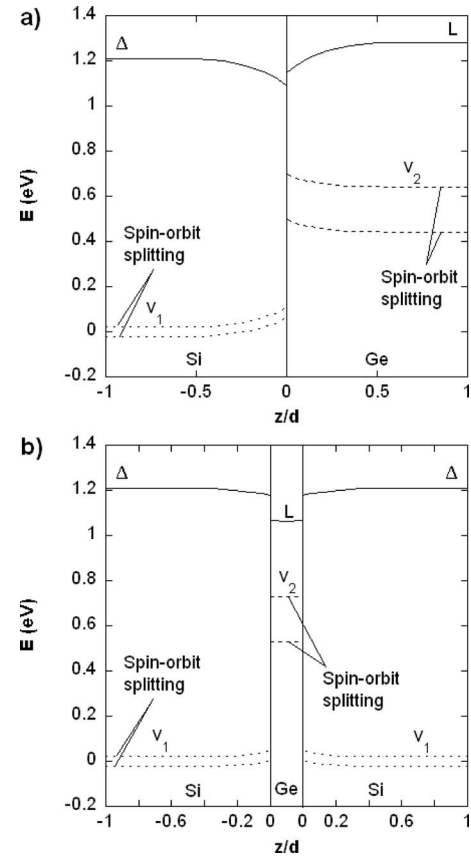


FIG. 10. Schematic of the band structure discontinuities predicted by deformation potential theory for (a) a 25 nm diameter Si/Ge biwire and (b) a 25 nm diameter Si/Ge/Si heterostructure with a 1 nm Ge layer (Ge layer thickness is not to scale). Energy levels are relative to the average of the v_1 valence band in Si.

the band structure in Si/Ge and Si/Ge/Si nanowire heterostructures. These results point to the need for more detailed theoretical studies, for example, using density functional theory, as well as for experimental determinations of the band structure changes at large strains.

Carrier confinement wells of the magnitude indicated in the present study are difficult to achieve in planar Si/Ge strained-layer structures without the introduction of interface defects. Thus these results imply that Si/Ge nanowire axial heterostructures can be used to tailor relatively deep carrier confinement regions near the interfaces, as well as shallower regions of localize strain-induced band-gap minima within specific locations in the interface as discussed above.

IV. CONCLUSIONS

A MEAM interatomic cross potential was developed for Si–Ge and shown to be accurate in MD models. Strain distributions in Si/Ge biwires of 10 and 25 nm diameter and a Si/Ge/Si heterostructure of 25 nm diameter with a 1 nm thick Ge layer were studied using MD. For biwires axial asymmetry and strain localization were observed in the in-plane strains at the Si/Ge interfaces. The strain maxima in the biwires were localized in a region of a few atoms in the case of the 10 nm diameter biwire and a region of a few nanometers in the case of the 25 nm diameter biwire. The strain in the Si/Ge/Si nanowire heterostructure was sufficient to reduce

the Ge band gap by more than a factor of 2 for a 1 nm thick Ge layer. Significant distortions in the height of the interfacial atoms across the interface are found for biwire heterostructures but not for the axial Si/Ge/Si disk structure. The distortions increase in curvature with decreasing biwire diameter. Strains in the biwire decrease sharply with distance from the interface and are confined to a region within 0.3 times the nanowire diameter, so band-gap modifications are closely localized to the interface layers for perfectly sharp interfaces. For the Si/Ge/Si heterostructures, the strain was relatively constant through the thickness of the 1 nm Ge layer. The results demonstrate that Si/Ge nanowire axial heterostructures have the potential for tailored band gaps, strong carrier confinement near the interfaces, and additional localized confinement in dots. Thus semiconductor strain engineering with nanowire heterostructures is shown to further extend band-gap engineering over that possible with strained-layer growth of planar structures.

ACKNOWLEDGMENTS

This research was funded by the Laboratory Directed Research and Development Program at Los Alamos National Laboratory. This work was performed, in part, at the Center for Integrated Nanotechnologies, a U.S. Department of Energy, Office of Basic Energy Sciences user facility (Contract No. DE-AC52-06NA25396).

- ¹R. People and J. C. Bean, *Appl. Phys. Lett.* **47**, 322 (1985).
- ²S. Luryi and E. Suhir, *Appl. Phys. Lett.* **49**, 140 (1986).
- ³S. Nakamura, M. Senoh, S. Nagahama, N. Iwase, T. Yamada, T. Matsushita, H. Kiyoku, H. Umeno, M. Sana, and K. Choco, *Appl. Phys. Lett.* **72**, 211 (1998).
- ⁴D. Zubia and S. D. Hersee, *J. Appl. Phys.* **85**, 6492 (1999).
- ⁵G. D. Watkins and J. W. Corbett, *Phys. Rev.* **138**, A543 (1965).
- ⁶G. D. Watkins, in *Deep Centers in Semiconductors*, edited by S. T. Pantelides (Gordon and Breach, New York, 1986), p. 147.
- ⁷J. W. Dailey, J. Taraci, T. Clement, D. J. Smith, J. Drucker, and S. T. Picraux, *J. Appl. Phys.* **96**, 7556 (2004).
- ⁸J. Taraci, M. J. Hytch, T. Clement, P. Peralta, M. R. McCartney, J. Drucker, and S. T. Picraux, *Nanotechnology* **16**, 2365 (2005).
- ⁹M. Menon, D. Srivastava, I. Ponomareva, and L. A. Chernozatonskii, *Phys. Rev. B* **70**, 125313 (2004).
- ¹⁰C. S. Moura and L. Amaral, *Nucl. Instrum. Methods Phys. Res. B* **228**, 37 (2005).
- ¹¹Y. M. Niquet, *Phys. Rev. B* **74**, 155304 (2006); Y. M. Niquet, A. Lherbier, N. H. Quang, M. V. Fernandez-Serra, X. Blasé, and C. Delerue, *ibid.* **73**, 165319 (2006).
- ¹²K.-H. Hong, J. Kim, S.-H. Lee, and J. K. Shin, *Nano Lett.* **8**, 1335 (2008).
- ¹³M. W. Larsson, J. B. Wagner, M. Wallin, P. Hakansson, L. E. Froberg, L. Samuelson, and L. R. Wallenberg, *Nanotechnology* **18**, 015504 (2007).
- ¹⁴E. Ertekin, P. A. Greaney, D. C. Chrzan, and T. D. Sands, *J. Appl. Phys.* **97**, 114325 (2005).
- ¹⁵G. Kästner and U. Gösele, *Philos. Mag.* **84**, 3803 (2004).
- ¹⁶S. Raychaudhuri and E. T. Yu, *J. Vac. Sci. Technol. B* **24**, 2053 (2006).
- ¹⁷See, for example, H. Liang, M. Upmanyu, and H. Huang, *Phys. Rev. B* **71**, 241403 (2005).
- ¹⁸J. Bardeen and W. Shockley, *Phys. Rev.* **80**, 72 (1950).
- ¹⁹W. H. Kleiner and L. M. Roth, *Phys. Rev. Lett.* **2**, 334 (1959).
- ²⁰H. Hasegawa, *Phys. Rev.* **129**, 1029 (1963).
- ²¹M. I. Baskes, *Phys. Rev. Lett.* **59**, 2666 (1987).
- ²²M. I. Baskes, *Phys. Rev. B* **46**, 2727 (1992).
- ²³J. G. Swadener, M. I. Baskes, and M. Nastasi, *Phys. Rev. B* **72**, 201202 (2005).
- ²⁴G. D. Watkins and J. W. Corbett, *Phys. Rev.* **134**, A1359 (1964).
- ²⁵S. Dannefaer, P. Mascher, and D. Kerr, *Phys. Rev. Lett.* **56**, 2195 (1986).
- ²⁶S. K. Estreicher, J. L. Hastings, and P. A. Fedders, *Phys. Rev. B* **57**, R12663 (1998).
- ²⁷R. F. S. Hearmon, *Adv. Phys.* **5**, 323 (1956).
- ²⁸F. W. Stillinger and T. A. Weber, *Phys. Rev. B* **31**, 5262 (1985).
- ²⁹J. J. Gilman, *J. Appl. Phys.* **31**, 2208 (1960).
- ³⁰R. J. Jaccodine, *J. Electrochem. Soc.* **110**, 524 (1963).
- ³¹Y. Wu, Y. Cui, L. Huynh, C. J. Barrelet, D. C. Bell, and C. M. Lieber, *Nano Lett.* **4**, 433 (2004).
- ³²N. Wang, Y. H. Tang, Y. F. Zhang, C. S. Lee, I. Bello, and S. T. Lee, *Chem. Phys. Lett.* **299**, 237 (1999).
- ³³V. T. Bublik, S. S. Forelik, A. A. Zaitsev, and A. Y. Poyakov, *Phys. Status Solidi B* **66**, 427 (1974).
- ³⁴A. Qteish and R. Resta, *Phys. Rev. B* **37**, 1308 (1988).
- ³⁵K. Mae, *Thin Solid Films* **395**, 235 (2001).
- ³⁶W. Wulfhekkel, B. J. Hattink, H. J. W. Zandvlet, G. Rosenfeld, and B. Poesema, *Phys. Rev. Lett.* **79**, 2494 (1997).
- ³⁷S. J. Plimpton, *J. Comput. Phys.* **117**, 1 (1995); <http://lammps.sandia.gov>.
- ³⁸F. H. Pollak and M. Cardona, *Phys. Rev.* **172**, 816 (1968).
- ³⁹I. Balslev, *Phys. Rev.* **143**, 636 (1966).
- ⁴⁰A. J. Read, R. J. Needs, K. J. Nash, L. T. Canham, P. D. J. Calcott, and A. Qteish, *Phys. Rev. Lett.* **69**, 1232 (1992).
- ⁴¹B. Delley and E. F. Steigmeier, *Appl. Phys. Lett.* **67**, 2370 (1995).
- ⁴²D. D. Ma, C. S. Lee, F. C. K. Au, S. Y. Tong, and S. T. Lee, *Science* **299**, 1874 (2003).
- ⁴³D. Shiri, Y. Kong, A. Buin, and M. P. Anantram, *Appl. Phys. Lett.* **93**, 073114 (2008).
- ⁴⁴J. Menendez and J. Kouvetakis, *Appl. Phys. Lett.* **85**, 1175 (2004).
- ⁴⁵J. Lim, X. Yang, T. Nishida, and S. E. Thompson, *Appl. Phys. Lett.* **89**, 073509 (2006).
- ⁴⁶L. D. Laude, F. H. Pollack, and M. Cardona, *Phys. Rev. B* **3**, 2623 (1971).
- ⁴⁷C. G. Van de Walle and R. M. Martin, *Phys. Rev. B* **34**, 5621 (1986).